*Progress In Electromagnetics Research, PIER 51, 295–328, 2005*

# A STUDY OF USING METAMATERIALS AS ANTENNA SUBSTRATE TO ENHANCE GAIN

**B.-I. Wu, W. Wang, J. Pacheco, X. Chen, T. Grzegorczyk and J. A. Kong**

Research Laboratory of Electronics
Massachusetts Institute of Technology
Cambridge, MA 02139-4307, USA

**Abstract**—Using a commercial software, simulations are done on the radiation of a dipole antenna embedded in metamaterial substrates. Metamaterials under consideration are composed of a periodic collection of rods, or of both rods and rings. The S-parameters of these metamaterials in a waveguide are analyzed and compared with their equivalent plasma or resonant structure. Farfield radiation is optimized by analytic method and is simulated numerically. The metamaterial is shown to improve the directivity.

## 1. INTRODUCTION

Recently, there has been growing interest in the study of metamaterials both theoretically and experimentally. Metamaterials are artificial materials synthesized by embedding specific inclusions, for example, periodic structures, in the host media [1–8]. Some of these materials exhibit either negative permittivity or negative permeability. If both permittivity and permeability of such materials are negative at the same frequency, then the composite possesses an effective negative index of refraction for isotropic medium[9] and is referred to as a left-handed metamaterial. The name is used because the electric field, the magnetic field and the wave vector form a left-handed system [9]. These metamaterials are typically realized artificially as composite structures that are composed of periodic metallic patterns printed on dielectric substrates.

One of the first theoretical studies was done by Veselago in 1960s [9]. He examined the propagation of plane waves in a hypothetical substance with simultaneous negative permittivity and permeability. He found that the Poynting vector of the plane wave is antiparallel to the direction of the phase velocity, which is contrary to the conventional case of plane wave propagation in natural media. It has been shown by Pendry et al. [10] that a medium constructed by periodic metallic thin wires behaves as a homogeneous material with a corresponding plasma frequency when the lattice constant of the structure and the diameter of the wire are small in comparison with the wavelength of interest [10]. Pendry et al. also showed that split ring resonators can result in an effective negative permeability over a particular frequency region [2]. Only a couple of years ago, Smith, Schultz, and Shelby from the University of California—San Diego constructed the first left-handed metamaterial in the microwave regime, and demonstrated the negative index of refraction [4].

Many properties and potential applications of metamaterials have been explored and analyzed theoretically. Pendry proposed that left-handed metamaterials could be used to build a perfect lens with sub-wavelength resolution [11]. Studies have been done on backward

waves propagation [12], waveguides [13, 14], Cerenkov radiation [15], resonators [16], etc.

We can view metamaterials as a broader class of materials than left-handed medium. It is a class of materials that enable us to manipulate permittivity and permeability. To this date, the technology in left-handed metamaterials is best suited for our purpose.

Little research has been done on applications of left-handed metamaterials in antenna systems. Emission in metamaterials using an antenna has been recently presented in 2002 by Enoch et al. [17]. Two features are of interest regarding the control of emission: direction and power of emission. Enoch et al. have demonstrated the feasibility of using a rod medium to direct the emission of an embedded source towards the normal of the substrate, thus confining the radiated energy to a small solid angle.

The metamaterial they used was a metallic mesh of thin wires. Such medium can be characterized by a plasma frequency [10]. The effective permittivity can be expressed as

$$\epsilon_p = 1 - \omega_p^2/\omega^2 \tag{1}$$

where $\omega_p$ is the plasma frequency and $\omega$ is the frequency of the propagating electromagnetic wave. From this equation, the effective permittivity is negative when the frequency is below the plasma frequency. When operating at the plasma frequency, the effective permittivity is zero, and hence yields a zero index of refraction ($n = \sqrt{\mu_r \epsilon_r}$). From Snell's law ($\sin\theta_t / \sin\theta_i = n_i/n_t$ where $i$ denotes the incident medium and $t$ denotes the transmitted medium), for $n_i \approx 0$, we obtain a $\theta_t$ of zero regardless of what $\theta_i$ is. As shown in Figure 1, if we place a dipole in a substrate with index of refraction $n \approx 0$, the exiting ray from the substrate will be normal to the surface.

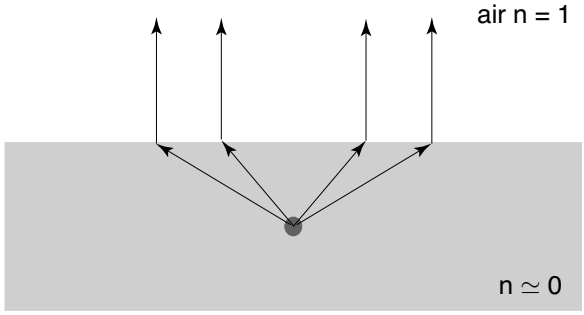


**Figure 1.** Dipole emission in a substrate with $n \simeq 0$.

Therefore, the closer the operating frequency is to the plasma frequency, the better the directivity. The permittivity just above the plasma frequency can be positive but still less than one. This will correspond to an index of refraction of less than one and close to zero. Then for any incident ray from inside such a medium to free space, the angle of refraction will be close to zero and the refracted rays will be close to normal. This property can be used to control the direction of emission. Inspired by Enoch, we propose to use left-handed like metamaterial (where the effective permittivity $\epsilon_{eff}$ and $\mu_{eff}$ will be zero at certain frequencies) as a substrate. Through the control of the structure's geometry, the frequencies where $\epsilon_{eff} = 0$ and $\mu_{eff} = 0$ can be tuned to the desired specification to produce directional emission in a wider band.

As it is mentioned above, thin wire structures can produce an effective negative permittivity below the effective plasma frequency and split ring resonators can result in an effective negative permeability over a particular frequency range. Overlaying these two frequency regions, both the permittivity and permeability are simultaneously negative, and thus the index of refraction may have a negative real value over a passband region. By manipulating the metamaterial structure, the effective permittivity and permeability can be changed individually, giving us the capability to control the position of the left-handed passband.

By using the commercially available software CST Microwave Studio®, studies will be done on a dipole embedded in metamaterial substrates. Methodology for studying antenna radiation in metamaterial substrates will be presented and results will be shown. The transmission property of a periodic rod medium will be analyzed from which an equivalent plasma model will be found. Dipole antenna radiation will be studied in the rod medium to establish our methodology.

## 2. PRIOR ART

Enoch et al. has used metamaterial as antenna substrate [17]. The metamaterial they used were layers of copper grids separated by foam. The copper grids has a square lattice with a period of 5.8 mm; each layer has a separation of 6.3 mm. This metamaterial possesses a (microwave) plasma frequency at about 14.5 GHz. The source of excitation used is a monopole antenna fed by a coaxial cable. The emitting part of the monopole is approximately centered at the center of the metamaterial substrate. In the experiment, a ground plane is added to the metamaterial substrate. At 14.65 GHz, it has the best

directivity.

The block of metamaterial substrate can be treated as a homogeneous material. Since it has a plasma frequency of approximately 14.5 GHz, the permittivity is closed to zero at this frequency, which means that the index of refraction is close to zero as well. From ray theory, the exiting ray from the substrate will be very closed to the normal of the substrate.

Changes in the copper grid metamaterial can only change where $\epsilon_{eff} = 0$ is. However, to obtain a index of refraction of $n = 0$, besides making permittivity zero, we can also let $\mu_{eff} = 0$. The known technology to manipulate both permittivity and permeability of a structure can be borrowed from the study of left handed metamaterials. In this section we will use rod medium as an example, since it is the simplest metamaterial and we have previous literature to compare our simulation results with. We will use similar aperture size for all our metamaterial substrates, and keep our region of interest in the microwave region. Ground planes will not be used in our simulation; the main effect will be that the beamwidth will be wider without the ground plane. In the next section, we will show the parameters used in the simulation of the metamaterials using CST Microwave Studio®.

## 3. METHODOLOGY

As discussed in the previous section, one of the objectives of this paper is to develop a methodology to analyze and design the metamaterial substrate for directive antenna. In this section, we will present the methodology in detail. The flow chart in Figure 2 shows the basic elements in our methodology and the process of analysis. We will use the rod medium as an example to illustrate how our methodology works, and further present how this approach can help us to examine and understand metamaterial as an antenna substrate. Additionally, this methodology can help us to optimize a metamaterial structure as substrate for directive antenna.

The metamaterial is the starting point of the analysis and is usually composed of periodic structures of metal and dielectric. We can build the structure and do experiments to see what the performance is as antenna substrate, or we can do numerical simulations. On the other hand, or we can do theoretical studies assuming the substrate is homogeneous. Experiment is the most expensive and time consuming, so we will use numerical simulation and theoretical studies to design a metamaterial structure that is good for antenna substrate. Since simulating the real size structure requires a lot of memory and takes a long time, we will put a slice of metamaterial in a parallel plate

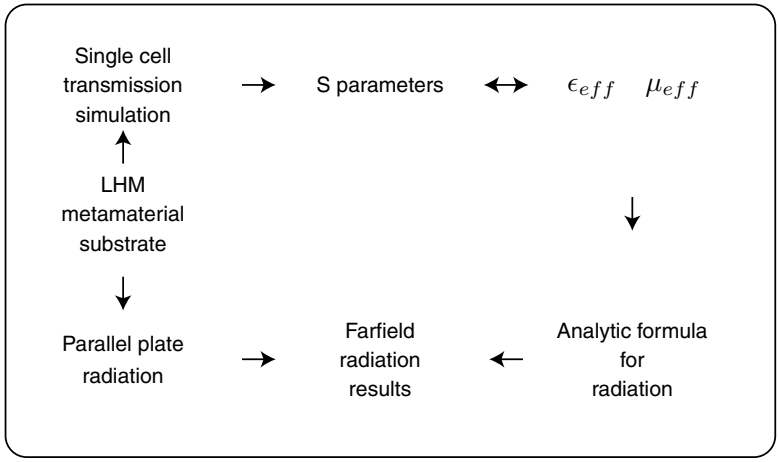


**Figure 2.** Methodology for analysis.

waveguide to approximate the radiation effect. We can also simulate the metamaterial in a waveguide and extract the S-parameters to find the effective $\mu$ and $\epsilon$ for all frequencies [18]. With the effective permittivity and permeability, we can use analytic formula to obtain farfield results with $\mu_{eff}$ and $\epsilon_{eff}$. The theoretical farfield result is faster to acquire than the ones from simulating in a parallel plate waveguide. Therefore, for optimizing, we will use theoretical method to find the optimized structure first, then simulate it in the parallel plate.

### 3.1. Simulation

For simulation, we use CST Microwave Studio® which is based on Finite Integration Technique (FIT) [19] for general purpose electromagnetic simulations. FIT applied to Cartesian grids in the time domain is computationally equivalent to the standard Finite Difference Time Domain (FDTD) method. For high frequency electromagnetic applications, time domain simulations methods are highly desirable, especially when broadband results are needed. FIT therefore shares FDTD's advantageous properties like low memory requirements and efficient time stepping algorithm. FIT combined with Perfect Boundary Approximation (PBA) can maintain the convenient structured Cartesian grids and permit an accurate modeling of curved structures [20].

The solver that we used for all our simulations is a transient solver.

For a wide frequency range, it uses only one computational run for the simulation of a structure's behaviors [20]. The version of CST Microwave Studio® that we are using is v4.2. We will be using it for radiation simulation and waveguide simulation.

### *3.1.1. Radiation Setup*

To illustrate the methodology in detail, a simple rod medium will be used as demonstration, which is very similar to what Enoch et al. has used [17]. The full size structure setup for the rod medium is shown in Figure 3. Each rod is a cylindrical Perfect Electric Conductor (PEC) structure that has a radius of 0.2 mm, and of length 250 mm. The period in the $x$ direction is 5.8 mm and in the $y$ direction is 6.3 mm. There are 6 layers of rods in the $y$ direction and 40 repetition in the $x$ direction. A 50 Ω S-parameter discrete port (dipole) of 1 mm in length

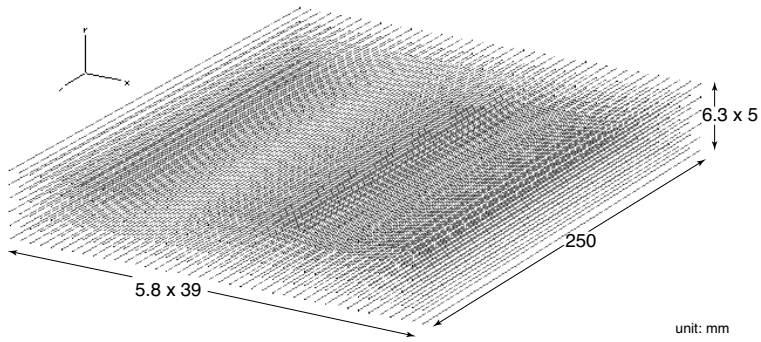


**Figure 3.** Full size rod structure.

is placed at the center of the structure for radiation. Mesh type of PBA (usually staircase type will be used if there is no curvature in the structure to save simulation time) is used with mesh density set at 10 lines per wavelength with refinement at PEC edges by 3. The resultant mesh in the $x$-$y$ plane is shown in Figure 4. How the mesh is setup is important to the accuracy of our simulation results. It should be fine enough to capture the details of the metamaterial structure. It is not as essential here for the simple rod medium as for some other structure which we will encounter later. The open boundary is modeled with Perfectly Matched Layer (PML) of 8 layers and a reflection coefficient of 0.0001. The automatic minimum distance to structure (when using "open (add space)" as the boundary condition)

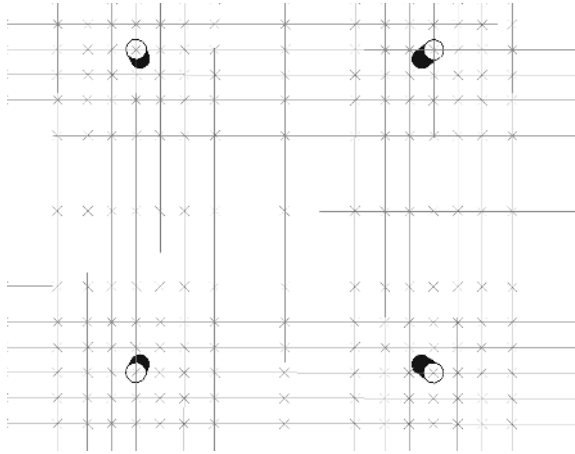

**Figure 4.** Mesh for full size rod structure.

is one wavelength. Farfield monitors are set up for frequencies from 11 GHz to 17 GHz. Radiation power are calculated at a distance 10 meters away from the excitation source (dipole in all our cases). These are the typical parameters we use in all our simulations, except for the mesh parameters and farfield monitor frequency range. Simulating the full size structure takes a lot of memory and as most metamaterial structures are more complicated than periodic rods, more time and even more memory are needed for simulation as well. Therefore, we use a slab of metamaterial in a PEC parallel plate waveguide to approximate the full size structure to save simulation time and memory. The slab setup is as shown in Figure 5. The dipole is again placed at the center of the structure. Mesh parameters are the same as before with the additional option of "Merge fix points on thin PEC and lossy metal sheets" chosen. All other parameters stay the same.

### *3.1.2. Waveguide Setup*

In order to study the metamaterial properties in a waveguide, a unit cell is identified from the full size structure and placed in a waveguide to collect the S-parameters. The unit cell for the rod medium is shown in Figure 6. The rod here is again modeled with PEC material, and the background as air. The top and bottom surface has PEC boundary conditions, whereas the left and right has perfect magnetic conductor (PMC) boundary conditions and front and back as open boundary condition. These boundary conditions will be the same for

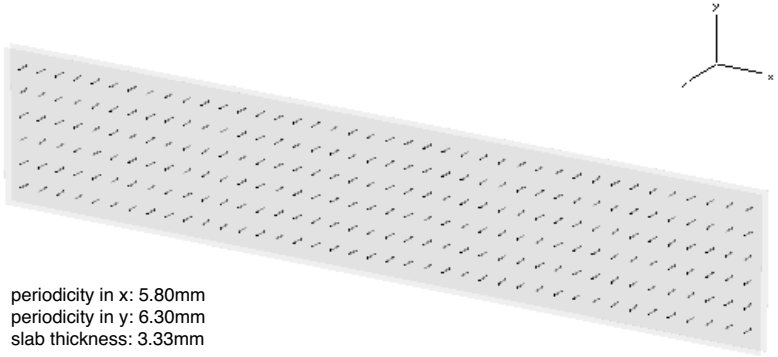


**Figure 5.** Slab of metamaterial (Rod structure between parallel plate waveguide with the $x$-$y$ plane being the plane of interest).

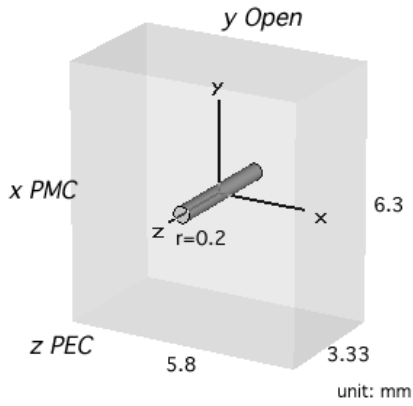


**Figure 6.** One cell rod structure in a waveguide.

all structures' unit cell that we presented in this paper. A waveguide port is placed at the open boundaries. Mesh density is 10 lines per wavelength; the options of refinement at PEC edges by factor 4 and inside dielectric materials are chosen. With the S-parameter data from the waveguide, we can retrieve the effective $\mu$ and $\epsilon$ at all frequencies [18]. An electric plasma frequency of 13.5 GHz is observed from retrieval (see Figure 7). Therefore, for farfield radiation, we will be interested in the frequencies around 13.5 GHz, as the index of refraction will be close to zero in that region, and therefore can possibly have

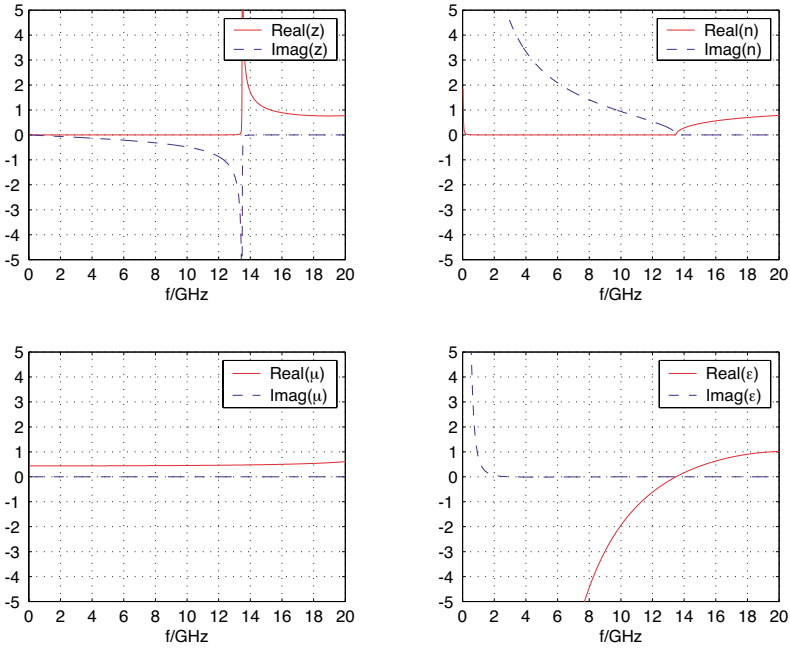


**Figure 7.** Retrieval results for rod medium.

beam sharpening effect. Using a rod medium, we can only have $\epsilon_{eff}$ to be zero at a certain frequency by changing the periodicity or the radius of the rods and thus making the index of refraction $n = 0$ at the corresponding frequency. Ultimately, our goal is to find a metamaterial structure where we can also get $\mu_{eff}$ to be zero at a frequency that is close to where $\epsilon_{eff} = 0$ is, so that the region where $n \approx 0$ can be broadened. Consequently we can potentially have a wider band where we can expect beam sharpening. Retrieval results ($\mu_{eff}$ and $\epsilon_{eff}$) enable us to relate metamaterials to a homogeneous material, and further assist us to estimate the radiation characteristic as we will demonstrate in the next section.

### 3.2. Analytical Method for Farfield Radiation

Consider a slab with permittivity $\epsilon_1$ and permeability $\mu_1$ as shown in Figure 8. Given an embedded input linesource oriented in the $z$ direction at the origin, its electric field [1] can be expressed as the

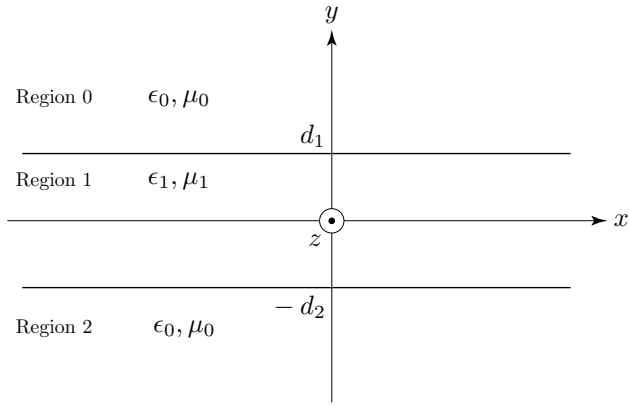


**Figure 8.** Configuration of a linesource in an infinite slab of thickness $d_1 + d_2$ with $\epsilon_1$ and $\mu_1$.

follows:

$$E_{iz} = \int_{-\infty}^{\infty} \mathrm{d}k_x \mathrm{e}^{\mathrm{i}(k_x x \pm k_{1y} y)} E_{\ell in} \tag{2}$$

where

$$E_{\ell in} = \frac{-\omega \mu_1 I}{4\pi k_{1y}} \tag{3}$$

is the spectrum which corresponds to the source at $x = 0$, $y = 0$ with magnitude $I$. The transmitted electric fields in the different regions then can be expressed as follows:
In region 0,

$$E_{0z} = \int_{-\infty}^{\infty} \mathrm{d}k_x E_{\ell in} (T_1 \mathrm{e}^{\mathrm{i}k_{0y} y}) \mathrm{e}^{\mathrm{i}k_x x} \tag{4}$$

In region 1,

$$E_{1z} = \int_{-\infty}^{\infty} \mathrm{d}k_x E_{\ell in} (\mathrm{e}^{\pm \mathrm{i}k_{1y} y} + A\mathrm{e}^{\mathrm{i}k_{1y} y} + B\mathrm{e}^{-\mathrm{i}k_{1y} y}) \mathrm{e}^{\mathrm{i}k_x x} \tag{5}$$

In region 2,

$$E_{2z} = \int_{-\infty}^{\infty} \mathrm{d}k_x E_{\ell in} (T_2 \mathrm{e}^{-\mathrm{i}k_{0y} y}) \mathrm{e}^{\mathrm{i}k_x x} \tag{6}$$

By matching the boundary conditions for the tangential electric and magnetic fields at $y = d_1$ and $y = -d_2$, we can find the coefficients $T_1$, $T_2$, $A$, and $B$.

$$T_1 = -\frac{2\mathrm{e}^{\mathrm{i}(k_{1y}-k_{0y})d_1}p_{01}\left(1+\mathrm{e}^{\mathrm{i}2k_{1y}d_2}(-1+p_{01})+p_{01}\right)}{\mathrm{e}^{\mathrm{i}2k_{1y}(d_1+d_2)}(-1+p_{01})^2-(1+p_{01})^2} \tag{7}$$

$$T_2 = -\frac{2\mathrm{e}^{\mathrm{i}(k_{1y}-k_{0y})d_2}p_{01}\left(1+\mathrm{e}^{\mathrm{i}2k_{1y}d_1}(-1+p_{01})+p_{01}\right)}{\mathrm{e}^{\mathrm{i}2k_{1y}(d_1+d_2)}(-1+p_{01})^2-(1+p_{01})^2} \tag{8}$$

$$A = -\frac{\mathrm{e}^{\mathrm{i}2k_{1y}d_2}(-1+p_{01})\left(1+\mathrm{e}^{\mathrm{i}2k_{1y}d_1}(-1+p_{01})+p_{01}\right)}{\mathrm{e}^{\mathrm{i}2k_{1y}(d_1+d_2)}(-1+p_{01})^2-(1+p_{01})^2} \tag{9}$$

$$B = -\frac{\mathrm{e}^{\mathrm{i}2k_{1y}d_1}(-1+p_{01})\left(1+\mathrm{e}^{\mathrm{i}2k_{1y}d_2}(-1+p_{01})+p_{01}\right)}{\mathrm{e}^{\mathrm{i}2k_{1y}(d_1+d_2)}(-1+p_{01})^2-(1+p_{01})^2} \tag{10}$$

where

$$p_{01} = \frac{\mu_0 k_{1y}}{\mu_1 k_{0y}} \tag{11}$$

Using farfield approximation [21], the electric field in region 0 can be simplified as the follows:

$$E_{0z} = E_{\ell in}k_{0y}T_1\int_{-\infty}^{\infty}\mathrm{d}k_x\frac{1}{k_{0y}}e^{\mathrm{i}k_{0y}y}\mathrm{e}^{\mathrm{i}k_x x} = E_{\ell in}k_{0y}T_1\sqrt{\frac{2\pi}{ik_0 r}}\mathrm{e}^{\mathrm{i}k_0 r} \tag{12}$$

Normalizing this electric field to a free space case, we get

$$E_r = \frac{T_1}{p_{01}} \tag{13}$$

where $E_r$ denotes the relative electric field with respect to the free space case.

### 3.3. Radiation Results and Normalization

In this section, we will show all our different radiation results from different methods and how we compare them. Radiation results are plotted for the plane of interest, the $x$-$y$ plane, as shown in Figure 9 using a parallel plate radiation as an example. Angle $\phi$ is the angle from the $+x$ axis in the plane of interest. In the frequency band where index of refraction $n \approx 0$, the main beam (most power) is expected to occur at $\phi = 90^\circ$ and $\phi = 270^\circ$. We have different radiation results: simulation and analytic. These two methods plot different aspect of

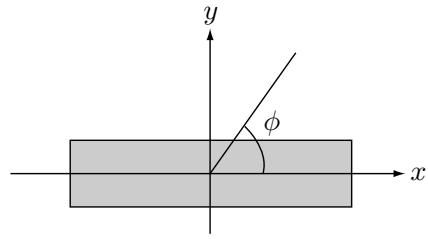


**Figure 9.** Radiation plane of interest.

farfield radiation, and we want to normalize them in some way such that we can compare our results.

The analytic method as shown in Section 3.2 calculates radiation using electric field from a linesource. The resultant farfield calculation is the ratio of the electric field with the metamaterial to the electric field in the free space case. It can then be squared to plot power in dB.

Simulation farfield radiation calculates the electric fields or power. In order to compare radiation results from these different methods, we need to find a way to normalize these data first. We noticed that in all these results, power is involved. In the analytic method, the power of each frequency is divided by the power of that frequency in the free space case. Therefore, for the same frequency, different power in different angles will be divided by the same number. However, if the frequency is different, the power will be divided by a different number. This tells us that there is a different scaling factor for different frequency. Looking at the gain results, all radiated power for each solid angle is divided by the input power, which is also frequency dependent. Hence, our method for normalizing all radiation figure is that for each frequency, we calculate the average relative power and normalize all data in that frequency with that average. The 3 dB beamwidth calculation will not be affected by this normalization.

Figure 10 shows the radiation results obtained from analytic method. From retrieval as discussed in Section 3.1.2, we expect to see directive radiation around the electric plasma frequency of 13.5 GHz. The frequencies with the most directive and highest power radiation are seen to center around at 13.6 GHz and 13.9 GHz respectively. Shortly after 13.9 GHz, the main beam starts to divert away from $\phi = 90°$, and form a "U" shape radiation pattern.

Next, we look at the radiation results acquired from simulation for both the full size and the parallel plate slab cases in Figure 11. For the full size structure simulation, the most directive beam is centered

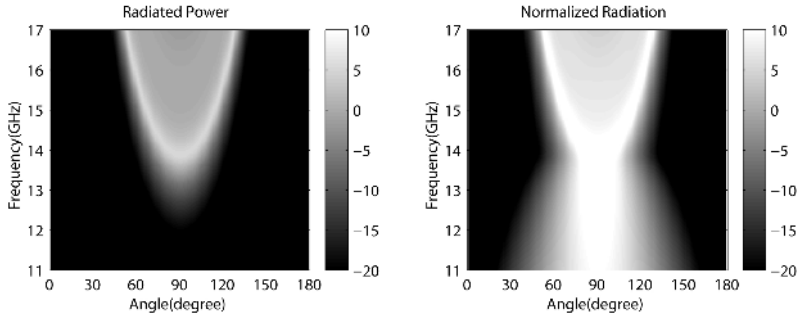


**Figure 10.** Radiated power and normalized radiation from analytic method for rod structure.

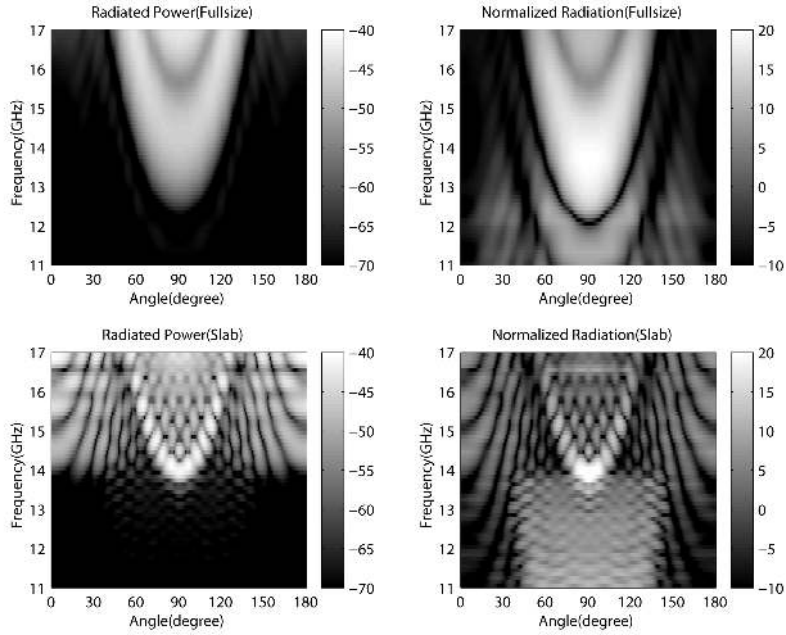


**Figure 11.** Radiated power and normalized radiation from simulation for rod (full size and slab structure).

at around 13.7 GHz and the high power beam is centered at around 14.4 GHz. Similarly to what the analytic results have predicted, the highest power beam takes place after the most directive beam, but with both these frequencies shift to slightly higher frequencies. The parallel

plate slab case exhibits a directive and high power beam at around 13.8 GHz and 13.9 GHz respectively. The parallel plate slab radiation has higher sidelobes which might be caused by the addition of the two PEC parallel plates. The two simulations are both a little bit different from what is predicted from the analytic method, however, they do demonstrate similar behavior of a "U" shape radiation pattern as the analytic case. We can conclude that our methodology has helped us to determine where directive and high power radiation will take place.

Besides power and directivity, we are also interested in the 3 dB beamwidth of the antenna system. The only beamwidth we are interested in is in the region where the index of refraction $n \approx 0$, and where the mainlobe of the radiation at one particular frequency is at $\phi = 90^\circ$ (normal to the substrate). Due to possible numerical simulation errors and approximations, we allow the main beam to be slightly away from the normal, given that the beam power at the normal direction is still within the 3 dB range of the main beam. We also allow the beam power to oscillate up and down as long as it is all within a 3 dB window. The bandwidth is decided by having the sidelobes to be 10 dB lower than the main beam, given that the beam in the normal direction is within 3 dB of the main beam. Figure 12 shows the maximum power angle at different frequencies and the corresponding 3 dB beamwidths for the full size rod structure;

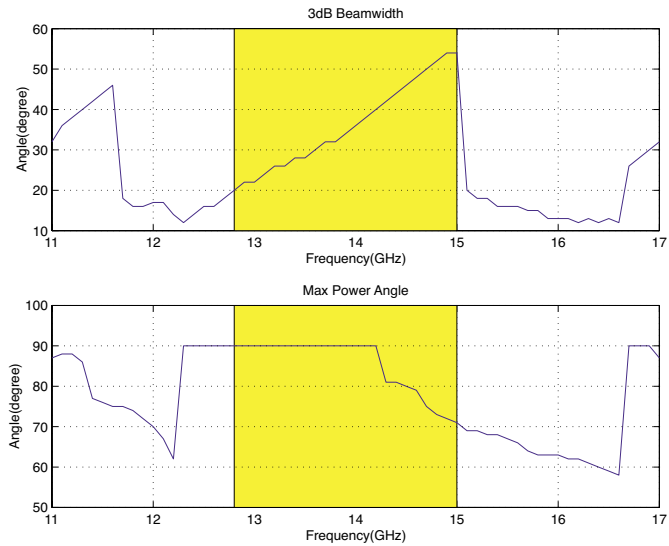


**Figure 12.** Beamwidth for full size rod medium.

interested bandwidths are the shaded regions. The smallest beamwidth of 20° occurs at 12.8 GHz, and the bandwidth is from 12.8 GHz to 15 GHz. Figure 13 shows the figures for the parallel plate slab case, where the smallest beamwidth of 6° happens at 13.7 GHz, and the bandwidth is from 13.7 GHz to 14 GHz.

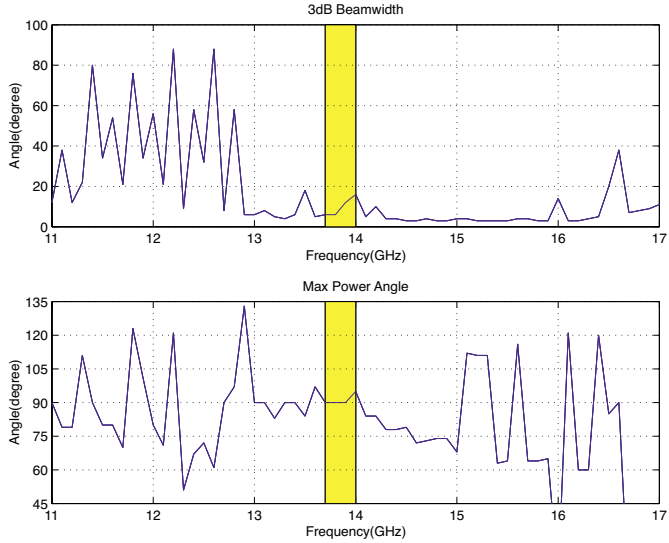


**Figure 13.** Beamwidth for slab of rod medium.

## 4. COMPARATIVE STUDY OF DIFFERENT METAMATERIAL SUBSTRATE

In this section, we will study several published metamaterial structures as antenna substrate. For each structure, the dimensions of a unit cell will be illustrated. Next, the effective permittivity and permeability will be obtained from the retrieval method based on the S-parameter scattering simulation in a waveguide.

These structures are all left handed metamaterials, there will be a region where $n < 0$ and the index of refraction $n = 0$ would occur at the frequencies where either $\epsilon_{eff} = 0$ or $\mu_{eff} = 0$. We are going to evaluate these different structures and see which one would work best for our purposes. Ideally, we would like to find a structure which is easy for tuning and manufacturing; then, we would optimize the structure such that it will have the desired properties at around 10 GHz.

At the end of this section, a summary of results and comparisons of these different structures will be presented.

### 4.1. 1-D Split-Ring Structure

2-D metamaterials are useful in the sense that it provides us with a relatively isotropic material property in the $x$-$y$ plane. However, construction of a rigid 2-D structure is difficult. 1-D structures are easier to fabricate and construct. The unit cell dimension is as shown in Figure 14.

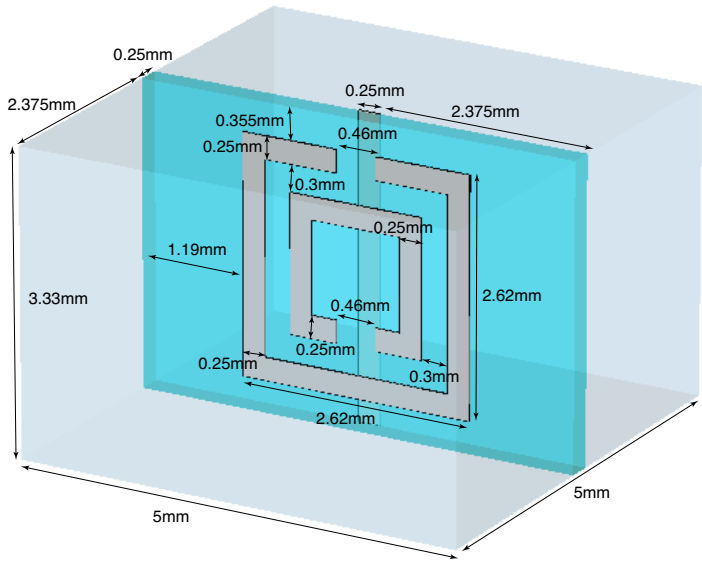


**Figure 14.** Unit cell 1-D Split-Ring structure in a waveguide.

The retrieval results are shown in Figure 15. Although the 2-D version of the same structure exhibit a usable left-handed band, The 1-D version has a larger rod spacings and has consequently pushed the electric plasma frequency too low. The split-ring structure also cause the left-handed band to shift from the stop band of the ring only structure, making it difficult to tune the $\epsilon_{eff}$ and $\mu_{eff}$ individually.

### 4.2. Symmetrical-Ring Structure

Another classic example of metamaterials is the symmetrical-ring structure [22]. The unit cell we used and its dimensions are as illustrated in Figure 16. We mainly scaled the original symmetrical-ring structure published in [22] in order for it to work in the microwave regime.

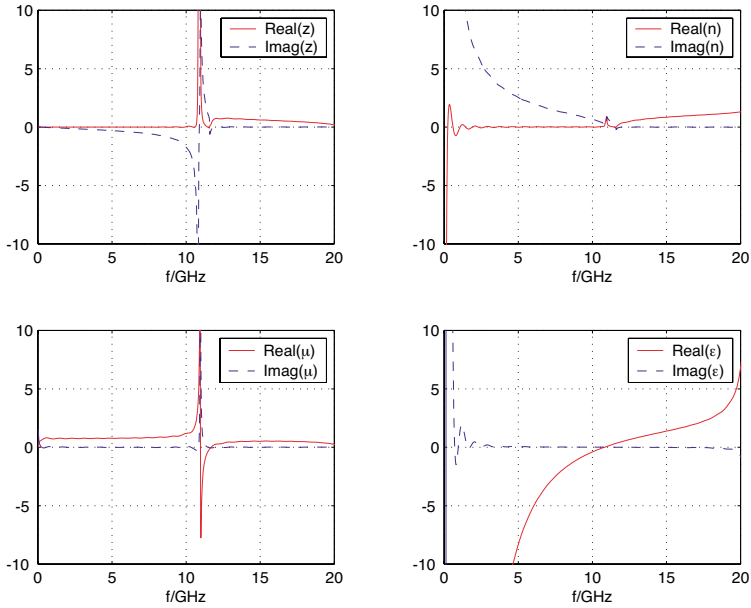


**Figure 15.** Retrieval results for 1-D Split-Ring structure.

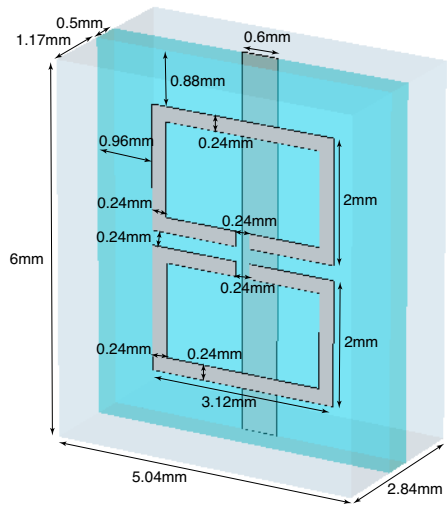


**Figure 16.** Unit cell Symmetrical-Ring structure in a waveguide.

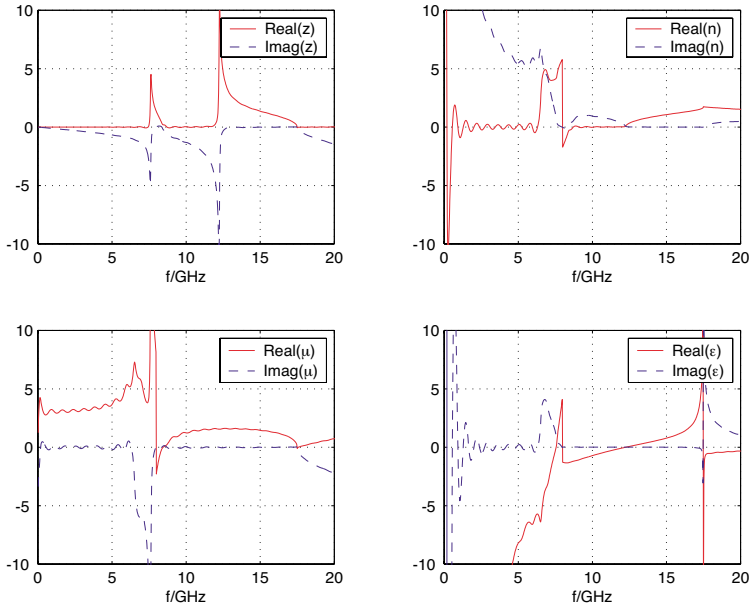


**Figure 17.** Retrieval results for Symmetrical-Ring structure.

With the S-parameters obtained from the PEC-PMC waveguide simulation, retrieval is done and shown in Figure 17. There is a resonant frequency at about 8 GHz. From 8.5 to 12 GHz, index of refraction $n \approx 0$, but the imaginary part of $n$ is slightly large. Therefore, instead of seeing directive radiation for all frequencies between this range, we might only have it around the two end frequencies. This structure, however, tends to yield clean retrieval response as there is less ringing effect from time-domain simulation. It would also allow us to tune $\epsilon_{eff}$ and $\mu_{eff}$ individually, because there is less coupling between the $\overline{E}$ field and the $\overline{H}$ field.

### 4.3. Omega Structure

Recently, there are also some new metamaterial structures being explored. One of which is an Omega-shaped structure [23]. The unit cell and its dimensions are presented in Figure 18.

The retrieval results for this Omega structure is shown in Figure 19. We can see that the retrieval results are not very clean for frequencies below 11 GHz. This might be caused by the increased complexity of the structure, since the rod are coupled with the rings,

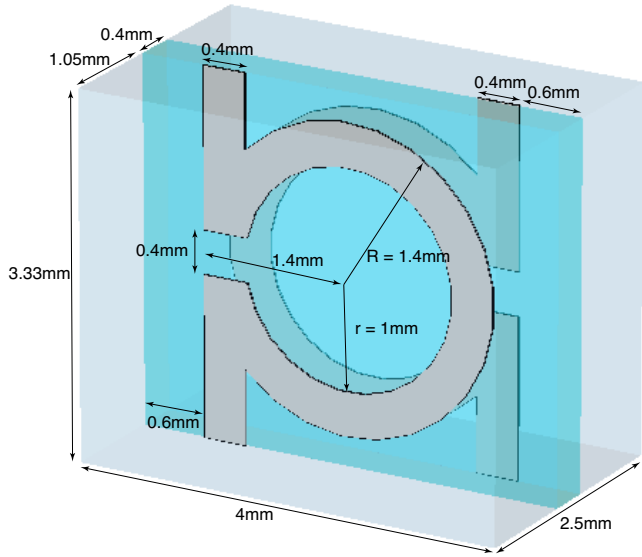


**Figure 18.** Unit cell Omega structure in a waveguide.

which means that the permittivity and permeability are coupled. However, we see that at around 11.4 GHz and 16.8 GHz, $n \approx 0$ and the imaginary part of $n$ is closed to zero, so we should be able to have regions where we observe directive radiation.

### 4.4. S Structure

Another novel metamaterial is a coupled "S" shaped structure [24]. There are no obvious ring or rod parts any more, but it still has the properties of having an electric plasma frequency and an magnetic resonant frequency. The unit cell is shown in Figure 20 and the corresponding retrieval results in Figure 21. Since the S structure does not have any curvature, the retrieval results are relatively clean. Similarly, S also have two frequencies where loss is low and $n \approx 0$. They are around 12.2 and 20 GHz, and index of refraction is approximately zero in between these two frequencies but the loss is large.

### 4.5. Summary

From studying and analyzing all these different metamaterial structures, Permittivity and permeability are coupled in the Omega

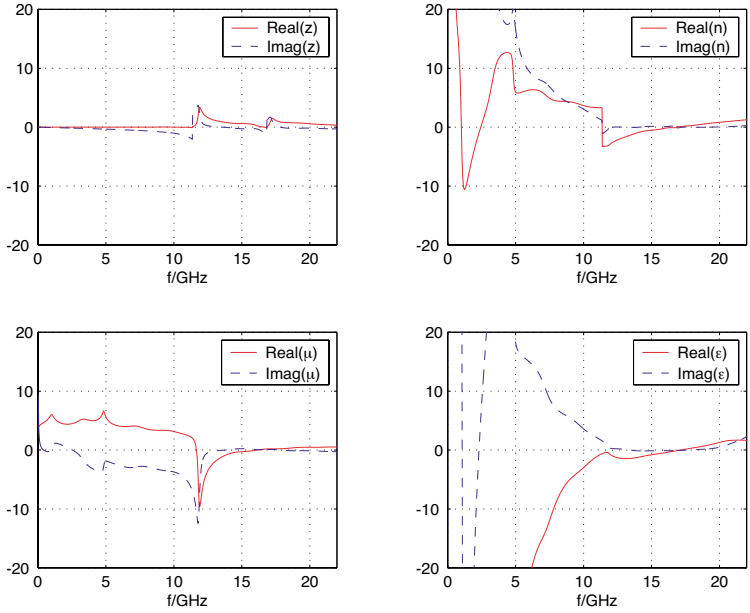


**Figure 19.** Retrieval results for Omega structure.

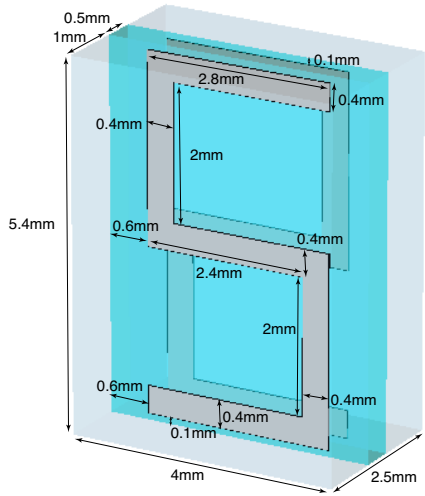


**Figure 20.** Unit cell S structure in a waveguide.

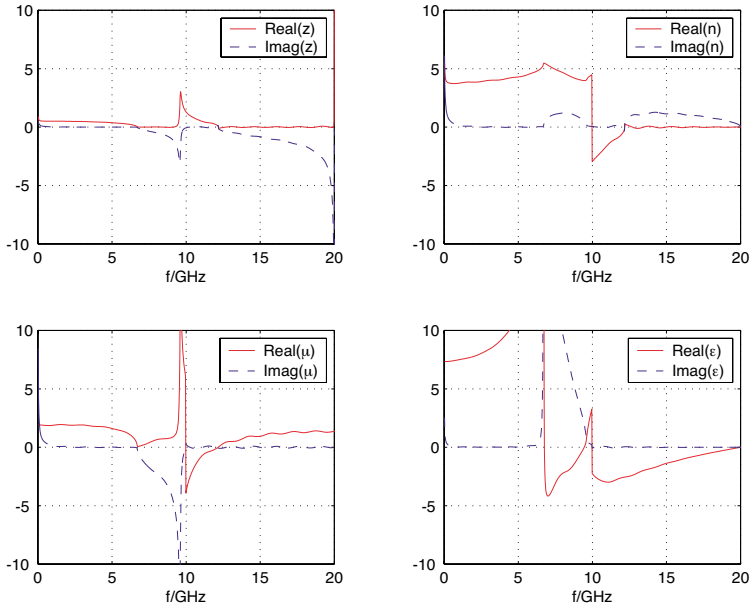


**Figure 21.** Retrieval results for S structure.

structure and the S structure, so these two structures would be harder to tune. The Symmetrical-Ring structure and the Split-Ring structure differ mainly in the implementation of their rings. The Symmetrical-Ring structure shows better directional beam and is easier to tune its permeability since its rings are symmetrical. For example, we can change the Symmetrical-Ring structure's ring dimensions while keeping the same gap while the Split-Ring ring consists of one bigger ring and one smaller ring, so if we make the bigger ring smaller then the gap would become smaller too unless we make the small ring smaller as well. Hence, more parameters are involved in the Split-Ring ring and therefore harder to tune. We are interested in the 8 GHz to 18 GHz frequency range, and in Table 1, we summarize how the different metamaterial structure perform as directive antenna substrate.

## 5. OPTIMIZED METAMATERIAL STRUCTURE

The symmetrical rings structure was first proposed in [22] for IR range. We choose to optimize this structure because of its simplicity to control $\mu$ and $\epsilon$ separately. It also has the main beam mostly along the normal direction, which is what we want for a directive antenna. We scale the

**Table 1.** Comparison among different metamaterial substrates.

| Structure | 1-D Split-Ring | Symmetrical-Ring | Omega | S |
|---|---|---|---|---|
| Bandwidth (GHz) | 12-12.3 | 16.1-18 | 13.7-14.1<br>15.6-17.2 | 10.7-10.8 |
| Retrieval | clean | clean | unclean | unclean |
| Tunability | medium | easy | hard | hard |

geometry to microwave regime and change some parameters in order to yield wider band, higher power, and smaller beamwidth. If we see from retrieval that there are two frequencies where the index of refraction $n = 0$, but far from each other, then the imaginary part of $n$ is usually too large (loss is large) for the frequencies in between to maintain high power.

Changes are made on top of the basic symmetrical rings structure to make where $\epsilon = 0$ and $\mu = 0$ closer to each other. Instead of having two small regions where we see high directivity and high power, we hope to have one larger region with high directivity and high power. For optimization, we carry out the one cell PEC-PMC waveguide simulation, and use the obtained S-parameters to retrieve the effective permittivity, permeability and index of refraction with which we calculate the analytic farfield radiation. If the analytic radiation result is not satisfactory, then the geometry of the unit cell will be further modified until the analytic radiation exhibits high power in a wider band with high directivity.

### 5.1. Optimized Geometry

The optimized final structure is shown in Figure 22. Retrieval results are shown in Figure 23. The two frequencies where $n = 0$ are very closed to each other. The imaginary part of $n$ is relatively small in between the two frequencies. Essentially, we have lowered the electric plasma frequency, and increased the magnetic resonance frequency. The electric plasma frequency is related to the size of the rods, and their periodicity. The smaller the period, the higher the electric plasma frequency. Therefore, by increasing the period of the unit cell, we also increase the period of the rod, and hence lowered the electric plasma frequency. As for magnetic resonance frequency, it is related to dimensions of the ring. Here we assume that the material property to be ideal: metal is still modeled with PEC, and the dielectric is lossless with a relative permittivity of 4. Changes in the material properties would cause changes in the effective permittivity and permeability as well.

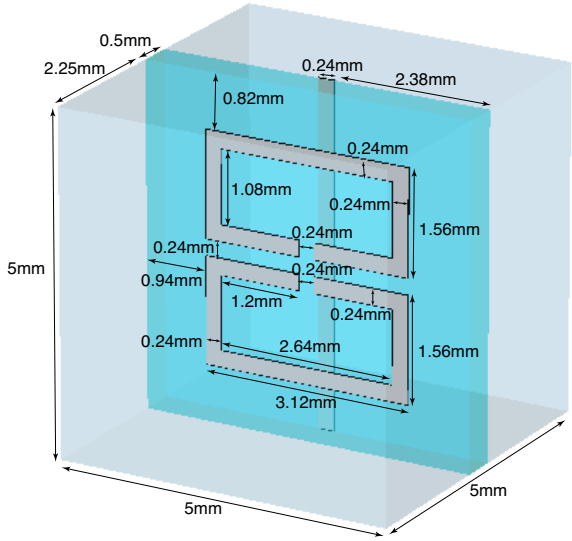


**Figure 22.** Unit cell of the optimized structure.

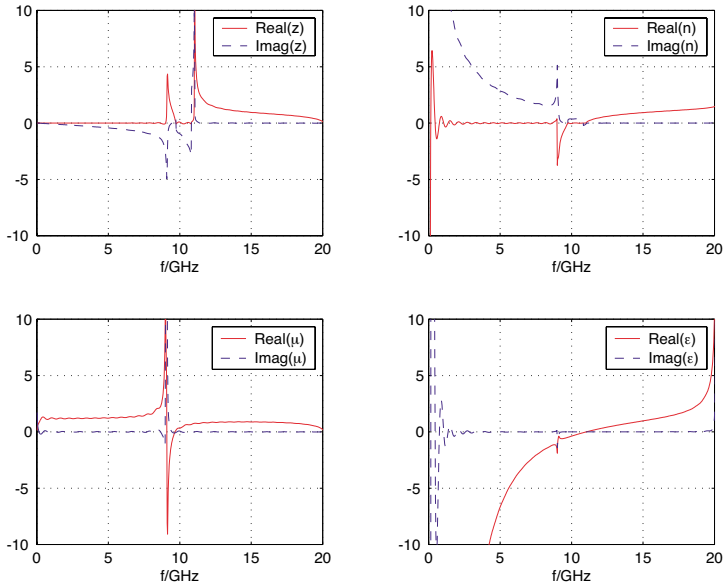


**Figure 23.** Retrieval results for final structure.

Retrieval results are shown in Figure 23.

Since this is a 1D structure, we can arrange it such that the dielectric align with either the $x$ direction or the $y$ direction as shown in Figure 24. We will refer to the one that has dielectric aligned in the $x$ direction as version $x$, and the other as version $y$.

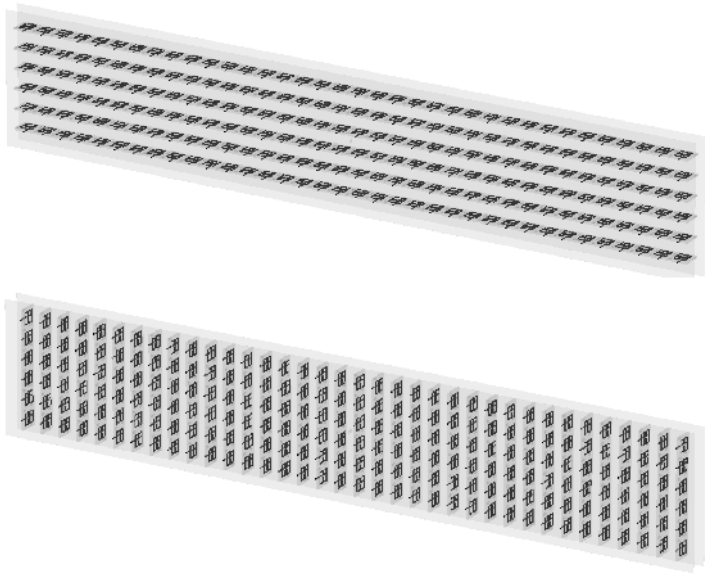

**Figure 24.** Two different 1-D orientation.

### 5.2. Radiation Results

We will first present the simulation result. The radiation results for the two orientations are presented in Figure 25, and the corresponding beamwidth results are shown in Figure 27 and Figure 26. As we can see, both of these structures are shown to have reasonable power, directivity (beamwidth) and bandwidth compared to other structures simulated in the previous section. Version $x$ has slightly higher power, and better directivity than version $y$.

To optimized the radiation, we also need to consider the antenna position. Is the position of antenna going to effect our radiation result? This is something that analytic method cannot tell us. Therefore, we can only run simulations to find out. For symmetry reason, there are two different antenna positions that we can explore which are shown in Figure 28. In Figure 29, the farfield radiation from the two different position of antenna are shown. One is always consistently 2 dB higher

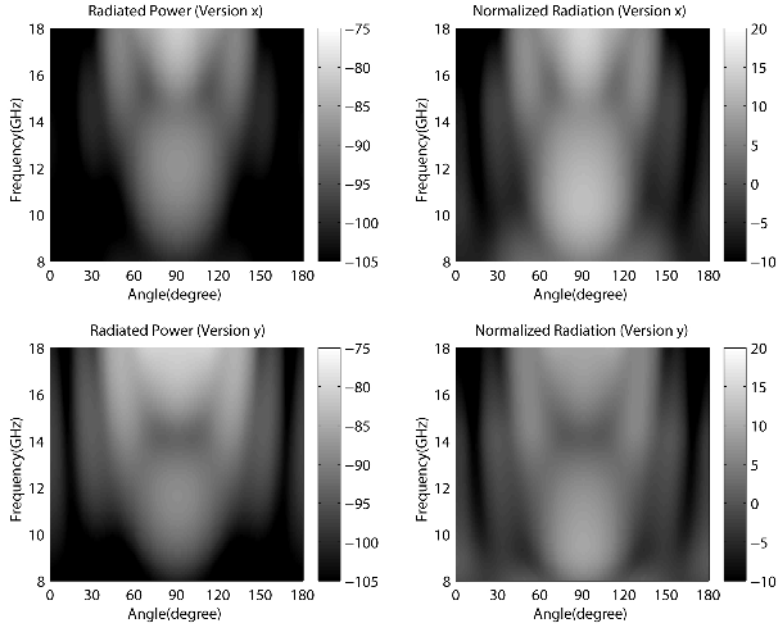


**Figure 25.** Radiated power and normalized radiation from slab simulation for version $x$ and version $y$.

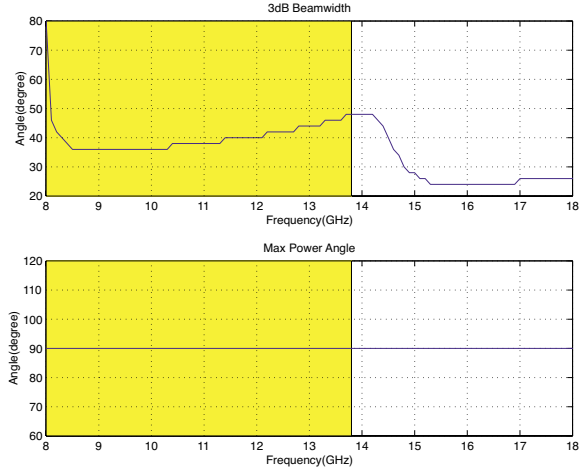


**Figure 26.** Beamwidth for version $x$ structure slab simulation.

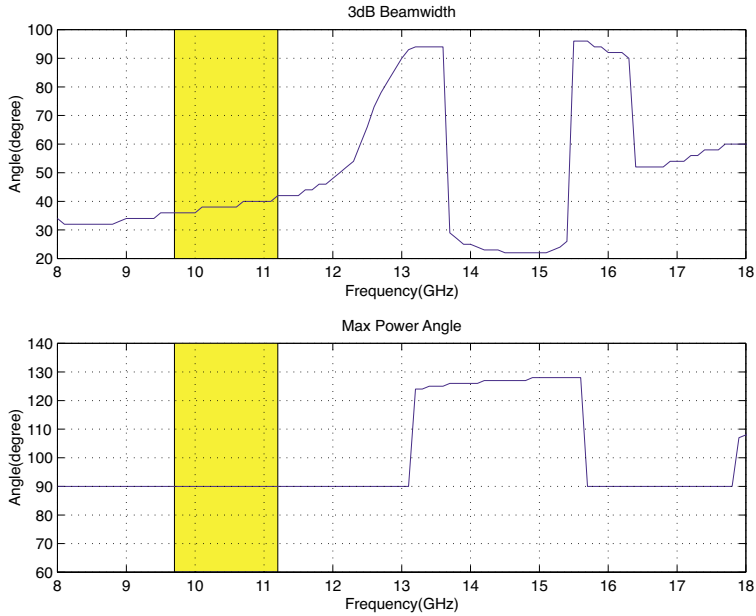


**Figure 27.** Beamwidth for version $y$ structure slab simulation.

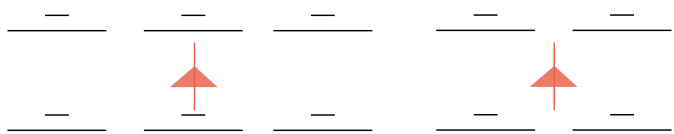

**Figure 28.** Two different antenna position.

than the other (varies between 2.06 to 2.37 dB). Therefore, for the metamaterial substrate, to obtain higher power radiation output, it is better to align the antenna with the boundary between two adjacent unit cells, and not with the rod of an unit cell.

We have been using an isotropic analytic method up to this point, we can modify and make it works for anisotropic case. Now the slab (shown in Figure 30) will be slightly different from what we see in Figure 8. The substrate permittivity and permeability will be expressed using tensors instead of scalers, which assumes isotropy.

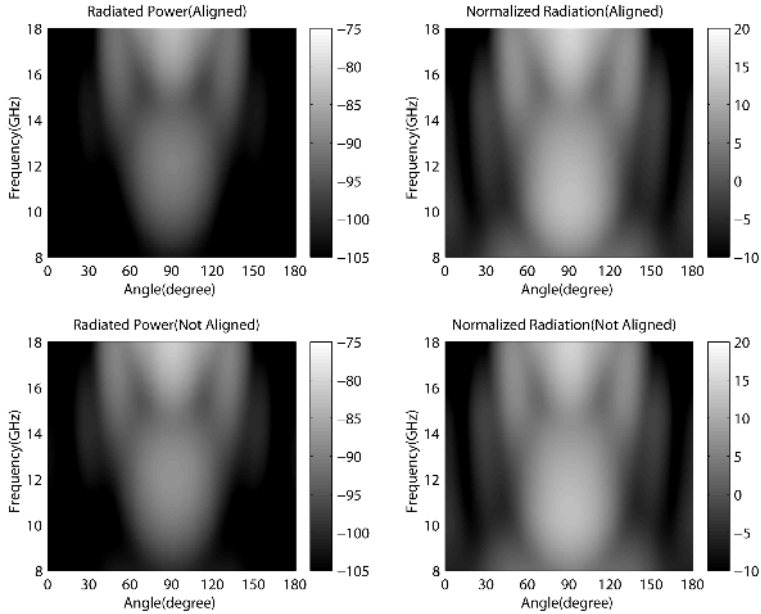


**Figure 29.** Radiated power and normalized radiation from slab simulation for different antenna positions.

Now the permittivity and permeability take the form

$$\bar{\bar{\epsilon}}_1 = \begin{bmatrix} 1 & 0 & 0 \\ 0 & 1 & 0 \\ 0 & 0 & \epsilon_z \end{bmatrix} \tag{14}$$

$$\bar{\bar{\mu}}_1 = \begin{bmatrix} \mu_x & 0 & 0 \\ 0 & \mu_y & 0 \\ 0 & 0 & 1 \end{bmatrix} \tag{15}$$

All the equations stay the same as shown in Section 3.2, except the expression for $E_{\ell in}$ and $p_{01}$.

$$E_{\ell in} = \frac{-\omega \mu_{1x} I}{4\pi k_{1y}} \tag{16}$$

$$p_{01} = \frac{\mu_0 k_{1y}}{\mu_{1x} k_{0y}}. \tag{17}$$

With this anisotropic analytic solution, the radiation for version $x$ and version $y$ are shown in Figure 31. They indeed look different from

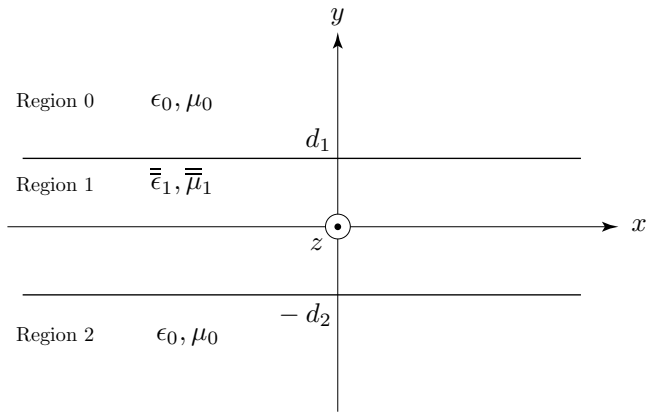


**Figure 30.** Configuration of a linesource in a slab with $\overline{\overline{\epsilon}}_1$ and $\overline{\overline{\mu}}_1$.

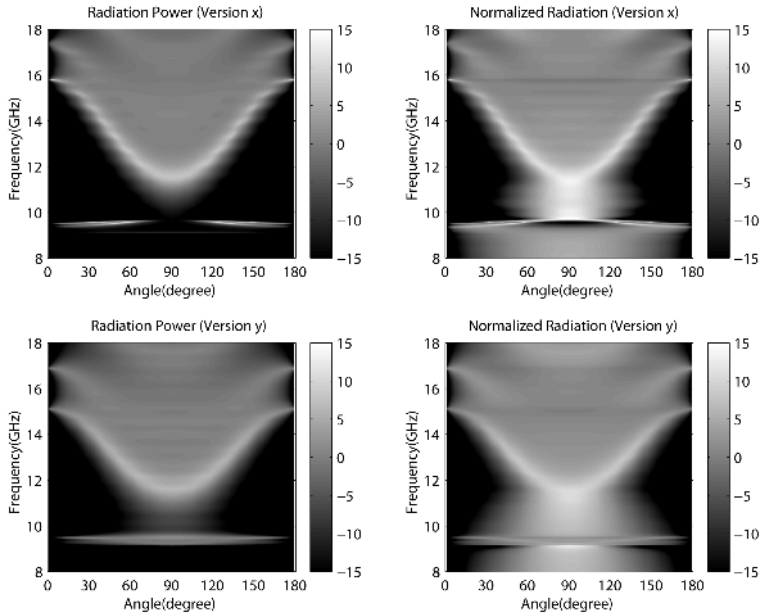


**Figure 31.** Radiated power and normalized radiation from analytic method for version $x$ and version $y$.

just using isotropic formula, and version $x$ does show better power and directivity than version $y$.

## 6. CONCLUSION

The goal of the project was to realize the manipulation of $\epsilon$ and $\mu$ through specific inclusion of metal in dielectrics to achieve a desired substrate properties in order to yield optimum radiation characteristics. Recent advances in Left-Handed Metamaterials (LHM) provided the technology to design and implement such structures. Combining analytic method for analyzing radiation for homogeneous anisotropic slab, optimization of structure becomes possible Hence LHM technology is adapted and optimized for metamaterial substrate design. We show that metamaterials can be approximated as being anisotropic homogeneous materials, not only in scattering (reflection/transmission) phenomenon, but also in embedded radiation. We also show that numerical simulation can address some design problems not possible with analytic method alone. The final structure to be tested is version $x$ with the dipole in the "Not aligned" position (aligned with the boundary of cells).

By modeling Metamaterials as homogeneous materials, we can simplify the design procedure and fine tune the radiation properties of the substrate. Retrieved parameters, upon using analytic formulas, match qualitatively with simulation results.

## REFERENCES

1. Kong, J. A., "Electromagnetic wave interaction with stratified negative isotropic media," *PIER*, Vol. 35, 1–52, 2002.
2. Pendry, J. B., A. J. Holden, D. J. Robbins, and W. J. Stewart, "Magnetism from conductors and enhanced nonlinear phenomena," *IEEE Trans. Microwave Theory Tech.*, Vol. 47, No. 11, 2075–2084, Nov. 1999.
3. Smith, D. R., W. J. Padilla, D. C. Vier, S. C. Nemat-Nasser, and S. Schultz, "Composite medium with simutaneously negative permeability and permittivity," *Phys. Rev. Lett.*, Vol. 84, No. 18, 4184–4187, May 2000.
4. Shelby, R. A., D. R. Smith, and S. Schultz, "Experimental verification of a negative index of refraction," *Science*, Vol. 292, 77–79, Apr. 2001.
5. Weiland, T., R. Schuhmann, R. B. Greegor, C. G. Parazzoli, A. M. Vetter, D. R. Smith, D. C. Vier, and S. Schultz, "*Ab initio*

numerical simulation of left-handed metamaterials: Comparison of calculations and experiments," *J. Appl. Phys.*, Vol. 90, No. 10, 5419–5424, 2001.

6. Parazzoli, C. G., R. B. Greegor, K. Li, B. E. C. Koltenbah, and M. Tanielian, "Experimental verification and simulation of negative index of refraction using snell's law," *Phys. Rev. Lett.*, Vol. 90, 107401, 2003.
7. Greegor, R. B., C. G Parazzoli, K. Li, and M. Tanielian, "Origin of dissipative losses in negative index of refraction materials," *Appl. Phys. Lett.*, Vol. 82, No. 14, 2356–2358, 2003.
8. Li, K., J. McLean, R. B. Greegor, C. G Parazzoli, and M. Tanielian, "Free-space focused-beam characterization of left-handed materials," *Appl. Phys. Lett.*, Vol. 82, No. 15, 2535–2537, 2003.
9. Veselago, V. G., "The electrodynamics of substances with simutaneously negative values of $\epsilon$ and $\mu$," *Soviet Physics USPEKHI*, Vol. 10, No. 4, 509–514, Jan.–Feb. 1968.
10. Pendry, J. B., A. J. Holden, D. J. Robbins, and W. J. Stewart, "Low frequency plasmons in thin-wire structures," *J. Physics-Condensed Matter*, Vol. 10, 4785–4809, 1998.
11. Pendry, J. B., "Negative refraction makes a perfect lens," *Phys. Rev. Lett.*, Vol. 85, No. 18, 3966–3969, Oct. 2000.
12. Lindell, I. V., S. A. Tretyakov, K. I. Nikoskinen, and S. Ilvonen, "BW–Media with negative parameters, capable of supporting backward waves," *Microwave Opt. Technol. Lett.*, Vol. 31, No. 2, 129–133, Oct. 2001.
13. Wu, B.-I., T. M. Grzegorczyk, Y. Zhang, and J. A. Kong, "Guided modes with imaginary transverse wavenumber in a slab waveguide with negative permittivity and permeability," *J. Appl. Phys.*, Vol. 93, No. 11, 9386–9389, June 2003.
14. Caloz, C., C.-C. Chang, and T. Itoh, "Full-wave verification of the fundamental properties of left-handed materials in waveguide configurations," *J. Appl. Phys.*, Vol. 90, No. 11, 5483–5486, 2001.
15. Lu, J., T. M. Grzegorczyk, Y. Zhang, J. Pacheco, B.-I. Wu, J. A. Kong, and M. Chen, "Cerenkov radiation in materials with negative permittivity and permeability," *Optics Express*, Vol. 11, No. 7, 723–734, Apr. 2003.
16. Engheta, N., "An idea for thin subwavelength cavity resonators using metamaterials with negative permittivity and permeability," *IEEE Antennas and Wireless Propagation Letters*, Vol. 1, No. 1, 10–13, 2002.

17. Enoch, S., G. Tayeb, P. Sabouroux, N. Guerin, and P. Vincent, "A metamaterial for directive emission," *Phys. Rev. Lett.*, Vol. 89, No. 21, 213902, Nov. 2002.
18. Chen, X., T. M. Grzegorczyk, B.-I. Wu, J. Pacheco Jr., and J. A. Kong, "An improved method to retrieve the constitutive effective parameters of metamaterials," Accepted for publication in *Phys. Rev. E.*
19. Weiland, T., "Time domain electromagnetic field computation with finite difference methods," *International Journal of Numerical Modelling*, Vol. 9, 259–319, 1996.
20. CST-Computer Simulation Technology, *CST Microwave Studio*® *Advanced Topics, Version 4*, 2002.
21. Kong, J. A., *Electromagnetic Wave Theory*, EMW, Cambridge, MA, 2000.
22. O'Brien, S. and J. B. Pendry, "Magnetic activity at infrared frequencies in structured metallic photonic crystals," *J. Physics-Condensed Matter*, Vol. 14, No. 25, 6383–6394, July 2002.
23. Huangfu, J., L. Ran, H. Chen, X. Zhang, K. Chen, T. M. Grzegorczyk, and J. A. Kong, "Experimental confirmation of negative refractive index of a metamaterial composed of $\omega$-like metallic patterns," *Appl. Phys. Lett.*, Vol. 84, No. 9, 1537–1539, Mar. 2004.
24. Chen, H., L. Ran, J. Huangfu, X. Zhang, K. Chen, T. M. Grzegorczyk, and J. A. Kong, "Left-handed metamaterials composed of only S-shaped resonators," to be published.

**Bae-Ian Wu** was born in Hong Kong on November 3, 1975. He received the B.Eng. degree in electronic engineering from the Chinese University of Hong Kong, Hong Kong, in 1997, the M.S. degree and Ph.D. in electrical engineering from Massachusetts Institute of Technology, Cambridge, Massachusetts, in 1999 and 2003. Since 1997 he has been a research assistant in the Department of Electrical Engineering and Computer Science and the Research Laboratory of Electronics at Massachusetts Institute of Technology, Cambridge, Massachusetts, where he has concentrated on electromagnetics wave theory and applications. He was a TA in the EECS department of MIT for several undergraduate and graduate EM courses (1998–2002). He is a currently a postdoctoral associate at Center for Electromagnetic Theory and Applications, Research Laboratory of Electronics, Massachusetts Institute of Technology.

**Weijen Wang** received her M.Eng. degree in 2004 from Massachusetts Institute of Technology, Cambridge, Massachusetts. Her research topic was designing directive antenna using metamaterial substrates. Since July 2004, she has been working on intellectual property.

**Joe Pacheco, Jr.** received the B.S. and M.Eng. degrees, in 2000, and the Ph.D. degree in 2004, all from the Massachusetts Institute of Technology in electrical engineering. From 2000–2004, he was a Graduate Research Associate at the Center for Electromagnetics Theory and Application at MIT. Currently, he is a Staff Member at MIT Lincoln Laboratory in the Systems and Analysis Group. He was a member of the administrative committee for the Progress in Electromagnetics Symposium (2000–2003). He is a member of the Eta Kappa Nu Association (since 1999), and a Member of the IEEE (since 2002). He was the recipient of the IEEE Microwave Theory and Techniques Society 2003 Graduate Fellowship Award.

**Xudong Chen** received his B.S. and M.S. degrees in Electrical Engineering in 1999 and 2001 from Zhejiang University, Hangzhou, China. Since September, 2001, he has been a research assistant with the Center for Center for Electromagnetic Theory and Applications, Research Laboratory of Electronics, Massachusetts Institute of Technology, USA. His research interests include electromagnetic inverse problem, metamaterial and mathematical modeling. In 1997 he won first prize in the Chinese National Mathematical Contest in Modeling.

**Tomasz M. Grzegorczyk** received his Ph.D. thesis from the Laboratoire d'Electromagnétisme et d'Acoustique (LEMA), Ecole Polytecnique Federale de Lausanne (Swiss Federal Institute of Technology, Lausanne) in December 2000. His research activities concerned the modeling of millimeter and submillimeter structures using numerical methods, as well as their technological realizations with the use of micromachining techniques. In January 2001, he joined the Research Laboratory of Electronics (RLE), Massachusetts Institute of Technology (MIT), USA, where he is now a research scientist. His research interests involve the study of wave propagation in complex media including left-handed metamaterials, the polarimetric study of ocean and forest, electromagnetic induction from spheroidal object for unexploded ordnances modeling, waveguide and antenna design, and wave propagation over rough terrains.

**Jin Au Kong** is a Professor of Electrical Engineering at the Massachusetts Institute of Technology. His research interest is in the area of electromagnetic wave theory and applications. He has published eight books, including *Electromagnetic Wave Theory* by Wiley Interscience, over 400 referred articles and book chapters, and supervised over 120 theses. He is Editor-in-Chief of the *Journal of Electromagnetic Waves and Applications*, Chief Editor of the book series *Progress in Electromagnetics Research*, and Editor of the Wiley Series in remote sensing.